



Article

A Novel Bifunctional Surface Coating Method to Effectively Eliminate Residual Li on NCM811 by Using Uniformly Dispersed Metal Oxide Solution

Seung Hyun Kim, Nanaaheb M. Shinde ID, Young-Eun Yun and Jeom-Soo Kim *

Department of Chemical Engineering (BK21 FOUR), DONG-A University, 37 Nakdong-daero, Saha-gu, Busan 49315, Republic of Korea; shkim0651@sk.com (S.H.K.); nanashinde2009@gmail.com (N.M.S.); eunyy@landf.co.kr (Y.-E.Y.)

* Correspondence: jsenergy@dau.ac.kr

Abstract: A uniformly coating transition metal oxide solution (TS-M) was developed to simultaneously remove residual Li compounds (RLCs) and stabilize the surface of NCM811 material. XRD analysis revealed that the synthesized cathode samples (TS-M, where M = Ti, Ge, Sn) exhibited hexagonal α -NaFeO₂ structures without impurity phases. FE-SEM and EDX results confirmed the formation of a uniform metal oxide coating (TS-Ti, TS-Ge: and TS-Sn) on the surface of NCM811, demonstrating its potential as a high-performance cathode material for lithium-ion batteries (LIBs). Among the treated samples, the TS-Sn sample delivered an excellent discharge capacity of 172.4 mAh g⁻¹ with a retention of 90.4% after 50 cycles at a 1.0 C rate, outperforming the TS-Ge and TS-Ti samples. Electrochemical impedance spectroscopy (EIS) further validated the improved impedance of NCM samples after Ti, Ge, and Sn coatings. Based on these findings, the application of Ti, Ge, and Sn metal oxide coatings to NCM811 is considered a reliable surface modification strategy for enhancing electrochemical performance by eliminating RLCs and stabilizing the surface.



Citation: Kim, S.H.; Shinde, N.M.; Yun, Y.-E.; Kim, J.-S. A Novel Bifunctional Surface Coating Method to Effectively Eliminate Residual Li on NCM811 by Using Uniformly Dispersed Metal Oxide Solution. *Batteries* **2024**, *10*, 453. <https://doi.org/10.3390/batteries10120453>

Academic Editor: Zhenzhen Wei

Received: 25 October 2024

Revised: 1 December 2024

Accepted: 6 December 2024

Published: 22 December 2024



Copyright: © 2024 by the authors. Licensee MDPI, Basel, Switzerland. This article is an open access article distributed under the terms and conditions of the Creative Commons Attribution (CC BY) license (<https://creativecommons.org/licenses/by/4.0/>).

Keywords: Lithium-ion battery; cathode; layered transition metal oxide; residual lithium compounds; surface coating

1. Introduction

Lithium-ion batteries (LIBs) have garnered significant attention as a suitable power source for electric vehicles (EVs), primarily due to their high energy density (50–260 Wh·kg⁻¹), extended cycle life (up to 10,000 cycles), low maintenance costs, and eco-friendly characteristics. With the expanding scope of EV applications, there has been a continuous increase in the demand for LIBs that offer enhanced safety and higher energy capacity [1–5]. In LIBs, the cathode plays a pivotal role in determining the overall capacity, power output, and lifespan of the battery. Cathode reactions are typically slower, and their capacity is smaller compared to anodes, which underscores the critical importance of optimizing cathode materials. Conventional cathode materials, such as LiCoO₂ and LiMn₂O₄, exhibit significantly lower specific capacities compared to their anode counterparts. This disparity represents a major obstacle in meeting the requirements for higher capacity and energy density necessary for advanced EV applications. As a result, improving the performance of cathode materials has emerged as a central focus in LIB research [1,6–8]. Layered LiNi_xCo_yMn_zO₂ (NCM, x + y + z = 1) is most widely used in LIBs because of their superior capacity and cost-effectiveness compared to other cathode materials, such as LiCoO₂ [9–16].

Over the last decade, numerous studies have demonstrated that increasing the nickel (Ni) content in NCM cathode materials is advantageous for enhancing specific capacity [17–20]. However, while a higher Ni content proportionally increases the specific capacity, it also introduces critical drawbacks such as cation mixing [9,20], structural degradation [13,21,22], and the formation of residual lithium compounds (RLCs) such as lithium hydroxide (LiOH)

and lithium carbonate (Li_2CO_3) [23]. Lithium hydroxide (LiOH), as an RLC, can cause significant issues during electrode slurry preparation by inducing gelation due to its high pH (>12) [24]. Meanwhile, lithium carbonate (Li_2CO_3) readily reacts with hydrofluoric acid (HF), which is generated by trace water in the electrolyte. This reaction not only produces gases that disrupt battery operation but also accelerates side reactions between the electrode and electrolyte [25]. HF formation, in turn, leads to the dissolution of transition metals from the cathode, resulting in surface corrosion, structural instability, and phase transformations that degrade the cathode's electrochemical performance [26].

Addressing these challenges and reinforcing the electrochemical performance of Ni-rich NCM cathodes requires the effective removal of residual Li from the material's surface. Significant efforts have been devoted to this goal. Among these, washing with deionized water has proven effective for removing residual Li but also risks dissolving Li from the layered structure, which causes rapid capacity loss [27,28]. An alternative approach is surface modification, which not only mitigates side reactions by forming a protective coating layer but also eliminates residual Li through chemical reactions. However, current surface modification techniques often result in non-uniform coatings thereby limiting their effectiveness in improving electrochemical performance. In this respect, it is necessary to develop a coating method that can effectively reduce the residual Li without compromising the structural integrity and electrochemical performance of Ni-rich NCM.

In this report, we propose a novel bifunctional surface coating method designed to simultaneously remove residual lithium compounds (RLCs) and stabilize the surface of NCM811 cathode materials for lithium-ion batteries (LIBs). Uniformly dispersed nanoparticles of transition metal oxides (Ti, Ge, and Sn) in isopropyl alcohol (IPA) were successfully synthesized using a hydrothermal method. These nanoparticles were selected as coating materials due to their superior properties, including high electrical conductivity, fast lithium-ion (Li^+) diffusion, high mobility, and low resistivity compared to commonly used oxides such as ZrO_2 , SiO_2 , MgO , TiO_2 , and Al_2O_3 . The Ti, Ge, and Sn nanoparticles effectively prevent side reactions, enhance structural and electrochemical stability, and maintain high conductivity. Furthermore, conventional coatings can increase interfacial resistance between the cathode material and the electrolyte, delaying Li^+ mobility during intercalation and deintercalation processes. This study provides an in-depth analysis of surface-modified NCM811 cathodes utilizing Ti, Ge, and Sn nanoparticles, examining their structural, morphological, and electrochemical properties. Advanced characterization techniques, including scanning electron microscopy (SEM), energy-dispersive X-ray spectroscopy (EDS), X-ray diffraction (XRD), and X-ray photoelectron spectroscopy (XPS), were employed to evaluate the quality and performance of the coating layers. The findings demonstrate the potential of this bifunctional coating method to improve the commercial viability and performance of Ni-rich NCM cathode materials for LIBs.

2. Materials and Methods

2.1. Material Preparation

All chemicals and solvents were obtained from commercial suppliers and used without further purification. To synthesize TS-M nanoparticles (M = Ti, Ge, and Sn), three transition metal precursors with high reactivity towards lithium were selected: titanium (IV) isopropoxide (TTIP, 97%, Sigma-Aldrich, Seoul, Republic of Korea), germanium (IV) isopropoxide (GeIP, 97%, Sigma-Aldrich, Seoul, Republic of Korea), and tin (IV) isopropoxide (TIP, 10% *w/v* in isopropanol). Isopropyl alcohol (IPA, 99%, Sigma-Aldrich, Seoul, Republic of Korea) and tetrabutylammonium hydroxide (TBAOH, 40% in water, Sigma-Aldrich, Seoul, Republic of Korea) were used as solvents and reagents. Commercial-grade $\text{LiNi}_{0.8}\text{Co}_{0.1}\text{Mn}_{0.1}\text{O}_2$ (NCM811, L&F, Daegu, Republic of Korea) was utilized as the target material for coating with the Ti, Ge, and Sn nanoparticles.

For the preparation of TS-Ti, the process involved the following steps:

[Preparation of Solutions]

Solution A was prepared by mixing 0.923 g of TTIP with 30 g of IPA.

Solution B was prepared by dissolving 0.212 g of TBAOH in 75 mL of distilled water.

[Synthesis of TBA-TiO₂ Compounds]

Solution A was slowly added to Solution B under continuous stirring at 400 rpm while heating at 150 °C for 2 h. During this step, a chemical reaction occurred between TBAOH and TTIP, resulting in the formation of TBA-TiO₂ compounds. This process ensured the homogeneous and uniform dispersion of TiO₂ particles in the reaction solution. Initially, the TBA-TiO₂ solution appeared as a yellowish turbid mixture, which transitioned to a transparent yellowish solution after several hours, indicating improved dispersion.

[Hydrothermal Treatment]

The pH of the TBA-TiO₂ solution was adjusted by adding 40 mL of distilled water, ensuring a controlled and stable pH. The solution was then transferred to a Teflon-lined autoclave and heated at 150 °C for 2 h in a box furnace. The resulting translucent solution contained uniformly dispersed TiO₂ nanoparticles, designated as TS-Ti.

A similar synthesis protocol was employed for the preparation of the Ge and Sn colloidal solutions, resulting in TS-Ge and TS-Sn nanoparticles, respectively.

To coat the surface of NCM811, the TS-M (M = Ti, Ge, Sn) compounds were homogeneously mixed with commercial-grade NCM811 under constant stirring for 10 min. The resulting slurry was filtered and dried at 120 °C for 8 h in a convection oven. The dried powder was subsequently heat-treated at 500 °C for 5 h under an oxygen atmosphere. The final surface-modified NCM811 samples, coated with the Ti, Ge, and Sn oxides, were labeled as TS-Ti, TS-Ge, and TS-Sn, respectively.

For comparison, a pristine NCM811 sample without surface modification was prepared. Additionally, to evaluate the effects of water washing on NCM811, a pristine sample was randomly washed with deionized (DI) water, denoted as W50.

2.2. Material Characterization

The crystal structures of the NCM811 samples were analyzed using X-ray diffraction (XRD, AERIS 300W, Malvern Panalytical, Malvern, UK) with Cu K α radiation ($\lambda = 1.5406 \text{ \AA}$). Field-emission scanning electron microscopy (FE-SEM, JSM-6700F, JEOL Co., Tokyo, Japan) was employed to examine the surface morphology of the resulting NCM811 particles. Energy-dispersive X-ray spectroscopy (EDS) was used to confirm the presence and uniformity of the coating material on the particle surfaces. Additionally, X-ray photoelectron spectroscopy (XPS, Thermo Fisher Scientific, Waltham, MA, USA) was performed using monochromatized Al K α radiation ($h\nu = 1486.6 \text{ eV}$) to investigate the oxidation states of the coating elements on the NCM811 surface. The total amount of residual lithium compounds, such as LiOH and Li₂CO₃, was quantified using the potentiometric titration system (Metrohm 888 Titrando, Herisau, Switzerland).

2.3. Electrochemical Measurements

The electrodes were prepared using a mixture of active material, carbon black (Super P), and polyvinylidene fluoride (PVDF) in a 90:5:5 weight ratio. The resulting slurry was uniformly applied onto aluminum foil and dried at 80 °C in a convection oven. The dried electrodes were then pressed and punched into disks with a diameter of 14 mm. These punched electrodes were further dried overnight at 120 °C under vacuum before being transferred to a glove box for cell assembly. The typical mass loading and density of the prepared electrodes were 12 mg·cm⁻² and 3.0 g·cm⁻³, respectively.

The fabricated cathode was assembled into CR2032 coin-type cells in an argon-filled glove box, with metallic lithium foil serving as the counter electrode. The electrolyte consisted of 1M LiPF₆ dissolved in a 3:7 volume ratio of ethylene carbonate (EC) and dimethyl carbonate (DMC). Galvanostatic electrochemical tests were conducted within a voltage range of 2.5–4.3 V (vs. Li/Li⁺) under various current densities at 25 °C and 45 °C. Electrochemical impedance spectroscopy (EIS) measurements were also performed

over a frequency range of 1 MHz to 10 mHz. These measurements were monitored in the discharged state both after formation cycles and following 50 charge–discharge cycles.

3. Results

To mitigate the RLC issue, two primary approaches were employed: (1) a washing process and (2) a lithium-reactive coating process. The washing process is effective at removing RLCs but comes with a significant drawback—the marked deterioration of cycle retention, as reported in previous studies [26–28]. In contrast, the lithium-reactive coating process is less efficient at RLC removal but compensates for this by forming a protective layer on the surface. This coating suppresses side reactions with the electrolyte thereby enhancing electrochemical performance and ensuring improved cycle stability, as demonstrated in earlier studies [24,29–32].

In this study, we propose a synergistic approach that combines the benefits of both methods into a multifunctional surface coating process. This dual-strategy approach not only addresses surface instability but also effectively reduces RLCs thus enhancing overall battery performance. A schematic representation of the proposed two-in-one concept is illustrated in Figure 1.

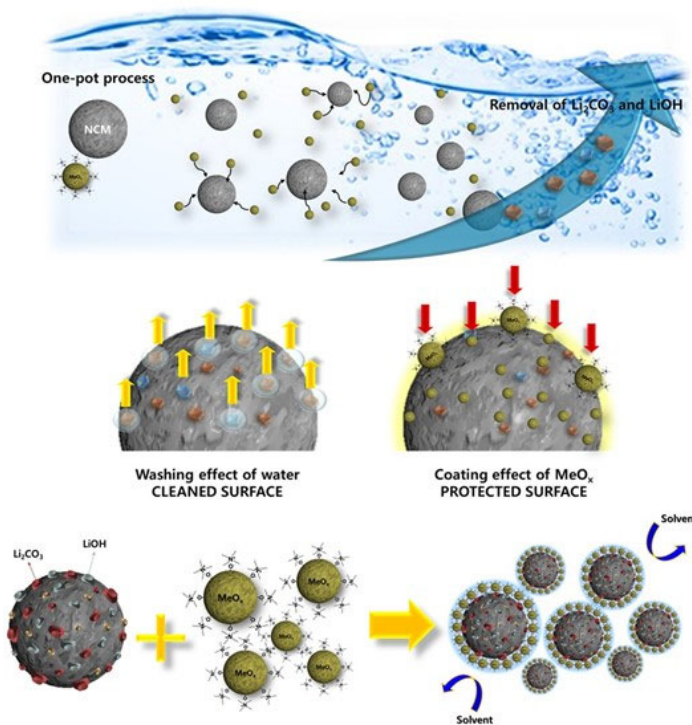


Figure 1. Schematic illustration for bifunctional coating process.

To mitigate the degradation associated with washing with water, a co-solvent system of IPA/H₂O was employed, which played a critical role in controlling adverse effects. Additionally, TBAOH was utilized as a dispersing agent to enable the systematic dispersion and settlement of metal oxide nanoparticles on the surface of the as-prepared NCM811. This innovative multifunctional hybrid coating process successfully produced M-coated NCM811 particles, representing a novel contribution of this work.

Figure 2a shows the XRD patterns of pristine W50 and TBA-M samples. The diffraction peaks correspond to the characteristic layered transition metal oxide structure based on a hexagonal α -NaFeO₂ framework with the space group R-3m. Notably, no additional peaks indicative of impurity phases were observed. The absence of reflections from the metal oxides is attributed to their minimal coating on the NCM811 surface.

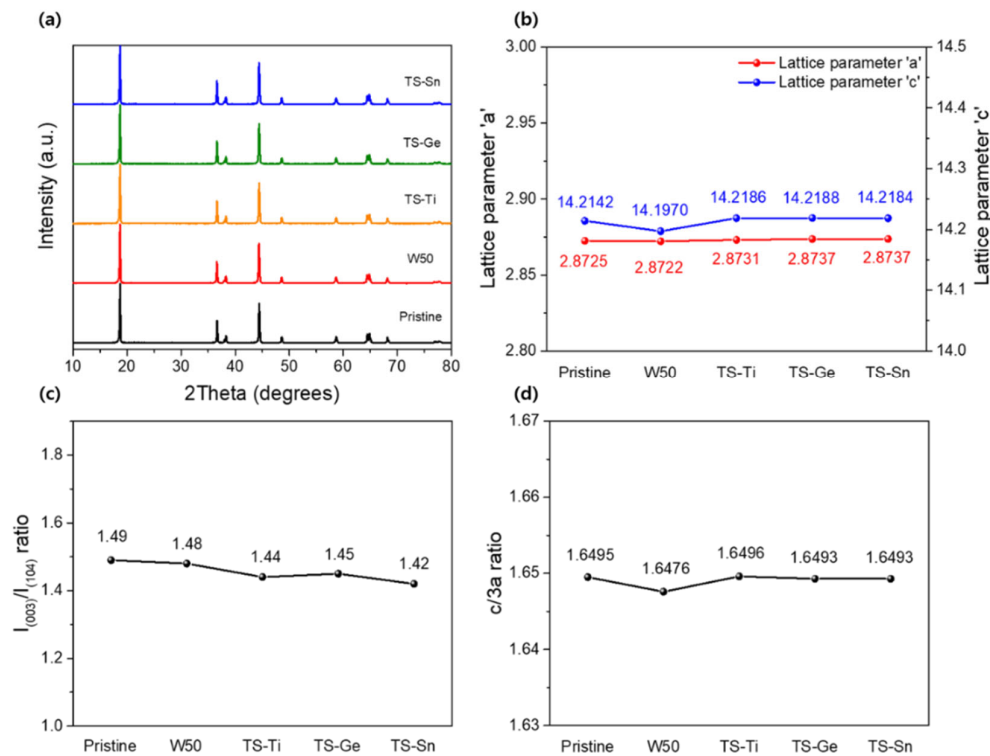


Figure 2. (a) XRD patterns, (b) lattice parameters a and c , (c) $I_{(003)}/I_{(104)}$ ratio, and (d) $c/3a$ ratio of pristine NCM811, W50, TS-Ti, TS-Ge, and TS-Sn cathode materials.

Lattice parameters for the TS-M particles were obtained through the XRD analysis, with the corresponding numerical presented in Figure 2b–d. The results confirm that no significant structural changes occurred after coating with metal oxides (Ti, Ge, and Sn), demonstrating that the original bulk structure of NCM811 remained intact. This highlights that the bifunctional coating process, which combines washing with a lithium-reactive treatment, effectively modified the surface of NCM811 without compromising its bulk structural integrity.

The surface morphologies of pristine and modified NCM811 particles were examined using field-emission scanning electron microscopy (FE-SEM), as shown in Figure 3. In Figure 3a,b, the pristine sample displays a rough and blurry surface layer, presumed to consist of lithium residual compounds (RLCs). The individual boundaries between primary particles are unclear or difficult to distinguish due to the presence of RLCs. In contrast, NCM811 particles subjected to post-treatment, such as washing with water or bifunctional coating, exhibit clear and smooth surfaces, indicating that residual lithium was effectively removed (Figure 3c–h). Notably, the TS-M samples, prepared with different metal sources (Ti, Ge, and Sn), demonstrate uniformly distributed small particles on the surface, which are assumed to be metal oxides (Figure 3e–h). These observations suggest that the bifunctional coating resulted in a uniform dispersion of metal oxide nanoparticles on the surface of NCM811. This uniform coating is expected to facilitate lithium-ion diffusion and enhance electron transfer during redox reactions. Energy-dispersive X-ray spectroscopy (EDS) mapping analysis was performed on the TS-M samples to confirm the presence of metal oxides, with the results presented in Figure 3i (i-1–i-3). As shown, Ti, Ge, Ni, Mn, Co, and Sn are uniformly distributed on the surface of the NCM811 particles.

To further evaluate the effects of the lithium-reactive coating, the concentration of RLCs in the pristine, W50, and TS-M samples was measured using potentiometric titration based on Warder's method [33]. According to the results presented in Figure 4, the residual lithium concentration in the pristine sample was approximately 11,960 ppm, attributed to the ambiguous boundaries between primary particles observed in the SEM images. In contrast, the W50 sample exhibited a significantly reduced lithium concentration of 2990 ppm,

corresponding to a 75% reduction. This demonstrates that washing with water effectively removed RLCs such as LiOH and Li_2CO_3 from the surface of the pristine NCM811.

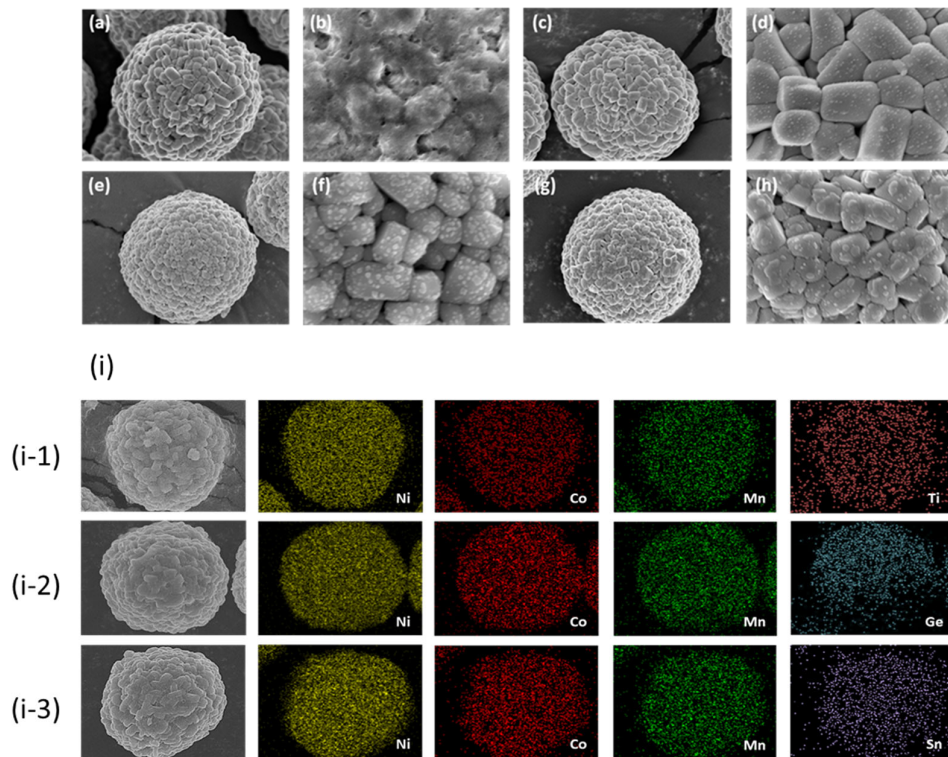


Figure 3. SEM images of pristine NCM811 (a,b), TS-Ti (c,d), TS-Ge (e,f), and TS-Sn (g,h). Corresponding EDS mapping analysis images (i): TS-Ti (i-1), TS-Ge (i-2), and TS-Sn (i-3), respectively.

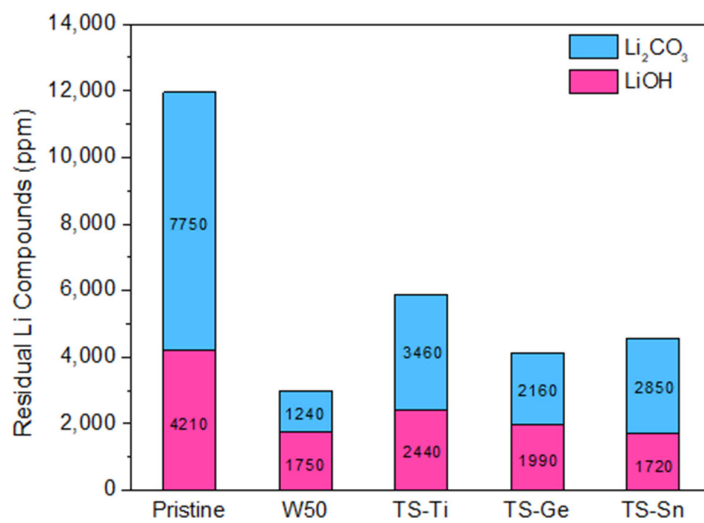


Figure 4. Residual Li concentrations of pristine, W50, TS-Ti, TS-Ge, and TS-Sn samples.

The lithium concentrations of the TS-M samples with different metal elements (Ti, Ge, and Sn) were also measured. The total residual lithium concentrations were reduced to approximately 3000–6000 ppm, representing reductions of 51% for Ti, 65% for Ge, and 62% for Sn. While these reductions are less significant compared to the 75% achieved with W50, they effectively demonstrate the ability of the TS-M coating process to remove RLCs.

X-ray photoelectron spectroscopy (XPS) was conducted to further investigate the surface condition of the resulting NCM811 particles. The XPS spectra for Ti 2p, Ge 3d, and Sn 3d levels are shown in Figure 5a–c. The Ti 2p spectrum (Figure 5b) exhibited peaks at

458.0 eV and 463.6 eV, corresponding to $\text{Ti} 2\text{p}_{3/2}$ and $\text{Ti} 2\text{p}_{1/2}$, respectively, indicative of Ti^{4+} in the form of TiO_2 [34,35]. Similarly, the Ge 3d spectrum (Figure 5c) showed peaks at 1218.6 eV, 1220.0 eV, and 124.9 eV [36–38], while the Sn 3d spectrum (Figure 5d) displayed peaks at 486.39 eV and 494.84 eV [39–41]. These results confirm that all three metals were present in the +4-oxidation state, existing as MO_2 , which is consistent with the titration results mentioned above.

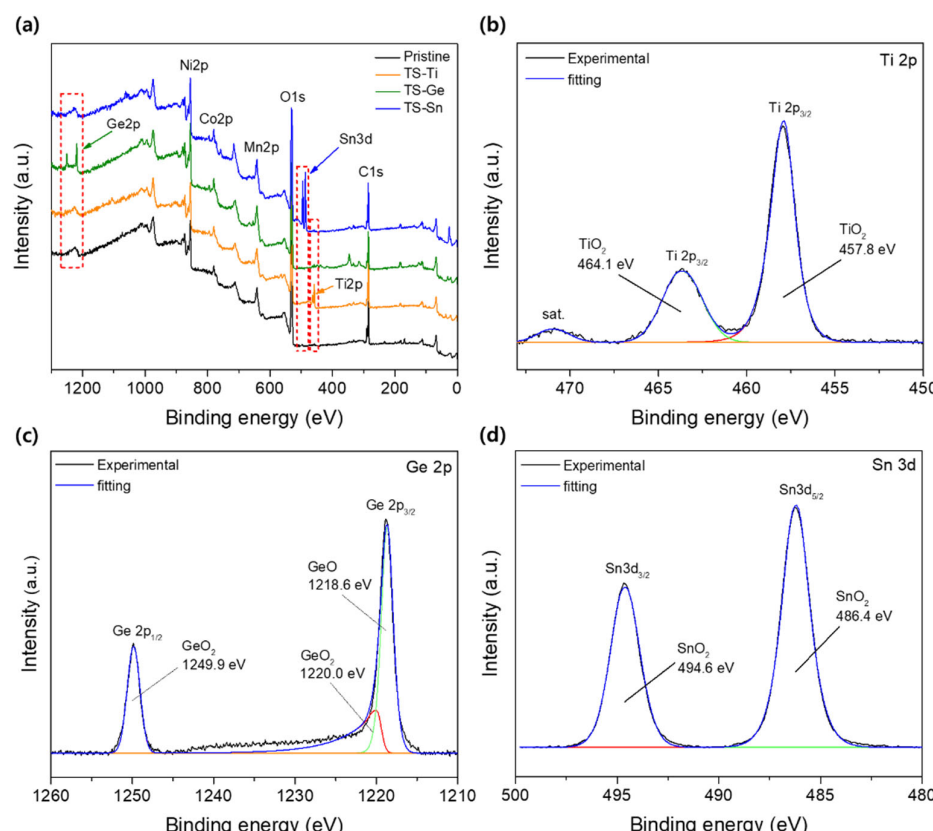


Figure 5. Survey XPS spectrum of pristine NCM811, TS-Ti, TS-Ge, and TS-Sn (a); and high-resolution XPS spectra of Ti 2p (b), Ge 2p (c), and Sn 3d (d) levels.

The detailed electrochemical properties of the prepared samples were evaluated in coin-cell configuration. Figure 6a presents the initial charge–discharge profiles of the pristine NCM811, W50, and TS-M samples with different metal elements (Ti, Ge, and Sn) over a voltage range of 2.5 to 4.3 V at a current density of 0.1C (20 mA g^{-1}). The initial discharge capacities of the pristine, W50, TS-Ti, TS-Ge, and TS-Sn samples were 206.2 mAh g^{-1} , 214.5 mAh g^{-1} , 209.5 mAh g^{-1} , 212.3 mAh g^{-1} , and 210.2 mAh g^{-1} , respectively. Among these, the W50 sample exhibited the highest discharge capacity, attributed to the removal of approximately 75% of the surface lithium, as confirmed by potentiometric titration. The TS-M samples showed increased initial discharge capacities compared to the pristine sample. Typically, surface coating with oxides decreases discharge capacity as oxides often impede lithium-ion diffusion and act as resistive layers at the electrode–electrolyte interface. However, in the TS-M samples, the discharge capacities increased despite the inert nature of TiO_2 , GeO_2 , and SnO_2 , likely due to enhanced kinetics resulting from the significantly reduced residual lithium.

Hence, the TS-M samples demonstrated improved capacity compared to the pristine sample. This electrochemical performance was attributed to the bifunctional coating, which simultaneously achieved two effects: (1) reducing residual lithium compounds (RLCs) on the surface through the washing process and (2) stabilizing the surface through a metal oxide coating, which acts as a protective layer against side reactions with the electrolyte [34,36,41,42]. To further evaluate the coating effects, the rate capabilities of the pristine, W50, and TS-M samples were tested at various current rates ranging from 0.5C

to 2.0C, as shown in Figure 6b. The TS-M samples exhibited better capacity retentions and higher discharge capacities compared to the pristine sample, despite the presence of a coating layer. At a 2.0C rate, the capacity retentions of TS-Ti, TS-Ge, and TS-Sn were 87.7%, 88.4%, and 88.1%, respectively, relative to their capacities at a 0.5C rate, slightly exceeding the pristine sample's retention of 87%. These results indicate that the surface coating with conductive materials prevents the buildup of resistance at the surface of the cathode materials thereby enhancing rate characteristics.

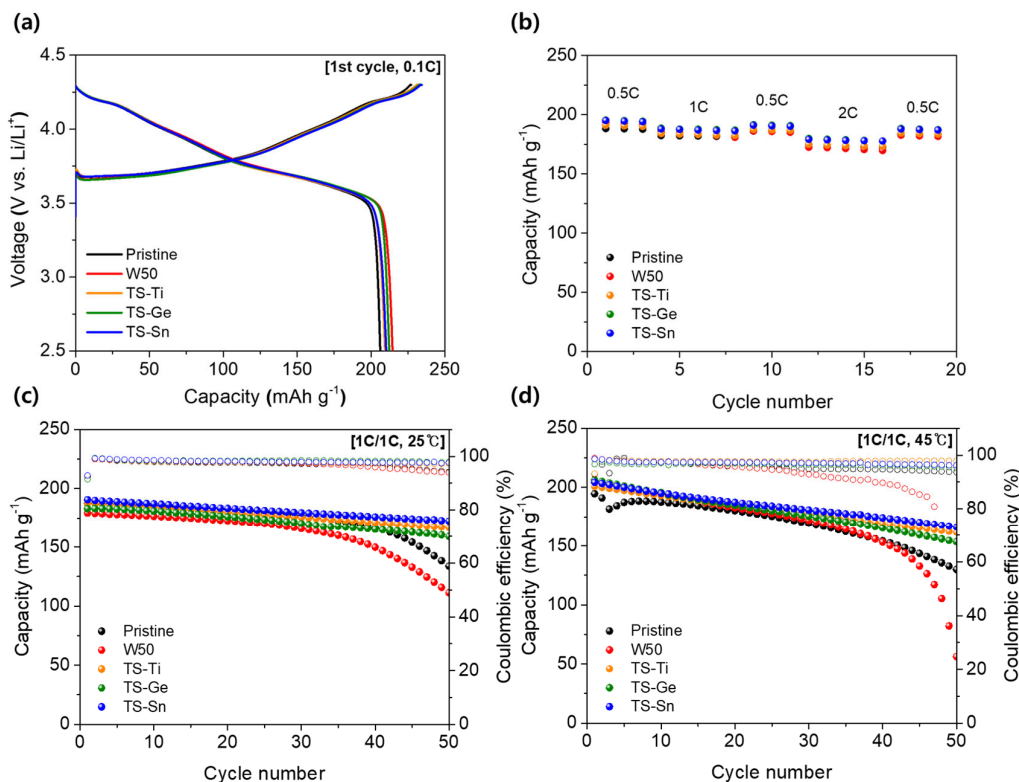


Figure 6. (a) Galvanostatic charge and discharge profiles of pristine, W50, and TSM (Ti, Ge, and Sn) at constant current of 0.1C. (b) Rate characteristics of all samples at 0.5C, 1.0C, and 2.0C. Cycling performance combined with coulombic efficiencies with current density of 1.0C(charge)/1C(discharge) at (c) 25 °C and (d) 45 °C.

To further investigate the effect of the bifunctional coating on electrochemical performance, cycling performance tests were conducted at various temperatures. Figure 6c illustrates the room temperature cycling performance at a constant current rate of 1.0C. After 50 cycles, the pristine sample exhibited a discharge capacity of 133.7 mAh g^{-1} with a capacity retention of 71.3%. While the W50 sample initially showed the highest discharge capacity, its capacity was dramatically decreased to show the lowest retention of 62.0% (111.3 mAh g^{-1} after 50 cycles). This reduced performance may be due to structural changes in the surface region during the washing process, where reactive Ni reacts with water to form a NiO rock salt phase, increasing surface resistance and deteriorating electrochemical performance [26–28]. In contrast, the TS-M samples (TS-Ti, TS-Ge, and TS-Sn) demonstrated significantly improved cycling performance compared to the pristine and W50 samples. After 50 cycles, the TS-Ti, TS-Ge, and TS-Sn samples exhibited discharge capacities of 166.6 mAh g^{-1} , 159.0 mAh g^{-1} , and 172.4 mAh g^{-1} , respectively, with capacity retentions of 88.6%, 86.8%, and 90.4%.

Elevated temperature cycling tests were conducted at 45 °C to evaluate the surface protection stability, as shown in Figure 6d. The pristine and W50 samples exhibited severe capacity fading, with capacity retentions of 66.7% and 27.5%, respectively, after 50 cycles. In contrast, the TS-Ti, TS-Ge, and TS-Sn samples showed much better cyclability, with

capacity retentions of 80.4%, 74.4%, and 81.3%, respectively. Among the TS-M samples, the TS-Sn sample exhibited the highest discharge capacity and capacity retention after 50 cycles at both room temperature and 45 °C. These results underscore the improved cycle performance resulting from the enhanced surface stability imparted by the multifunctional coating process.

To elucidate the reasons behind the improved cyclability and rate capability of the TS-M samples, electrochemical impedance spectroscopy (EIS) tests were conducted. Figure 7 presents the Nyquist plots for the pristine and TS-M samples after 50 cycles. All samples exhibited two distinct semicircles: the semicircle in the high-frequency range corresponds to the film resistance (R_f), while the semicircle in the mid-to-low-frequency range represents the charge transfer resistance (R_{ct}) at the cathode surface.

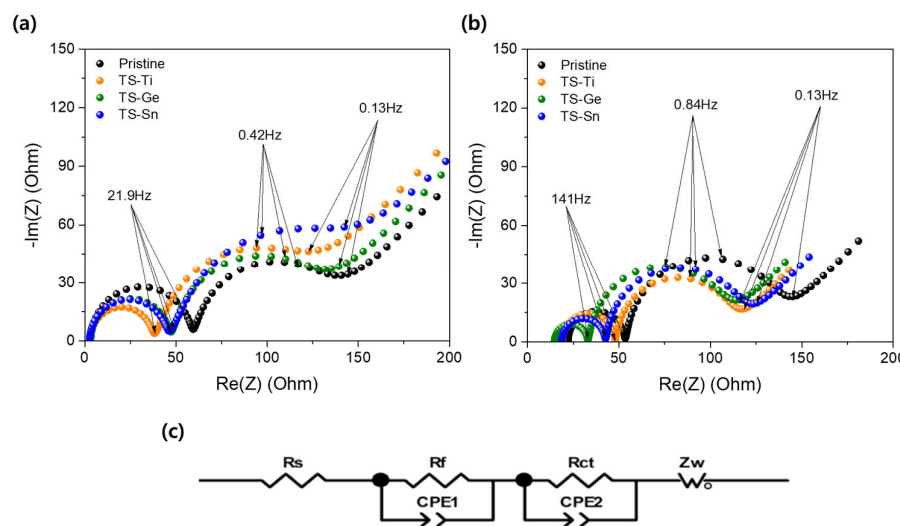


Figure 7. Nyquist plots of pristine and TS-M samples (a) before and (b) after 50 cycles; (c) equivalent circuit model used for fitting EIS spectra.

As shown in Figure 7a,b, the total impedance of the pristine sample is significantly larger than that of the TS-M samples both before and after 50 cycles. The TS-M samples displayed lower impedance during the initial cycle, attributed to the reduced resistance from the removal of residual lithium and enhanced electrochemical reactivity. After 50 cycles, the R_{ct} values for the TS-M samples remained smaller than those of the pristine sample although the R_{ct} values were increased for all samples. Notably, the R_{ct} of the pristine sample ($76.66\ \Omega$) was much larger than those of the TS-M samples: TS-Ti ($58.86\ \Omega$), TS-Ge ($67.91\ \Omega$), and TS-Sn ($68.39\ \Omega$). The EIS spectra were fitted using an equivalent circuit model (Figure 7c), comprising R_{ct} , R_f , and the corresponding constant phase element (CPE), providing further insight into the electrochemical processes. These trends of R_{ct} after 50 cycles are attributed to the minimized side reaction between cathode and electrolyte at the surface, achieved through the metal oxide coating. While the pristine sample showed greater degradation, the metal oxide coating layer on the TS-M samples effectively mitigated interfacial resistance caused by residual lithium and suppressed undesirable side reactions with the electrolyte thereby preserving the stability of NCM811.

4. Conclusions

In this study, the synergistic effect of a bifunctional coating using a metal oxide solution was demonstrated. A uniform coating layer of nano-sized metal oxides (Ti, Ge, Sn) was successfully applied to the surface of NCM811, introducing a novel surface coating method that ensures the uniform distribution of metal oxides on the active material. The cycling performance and rate capability of the TS-M samples were significantly improved by this bifunctional coating. Potentiometric titration confirmed that the concentration of residual lithium on the surface of the NCM811 particles was effectively reduced by a bifunctional

coating. The nano-sized metal oxides (Ti, Ge, Sn) contributed to reduced charge transfer resistance due to the uniform distribution of transition metal oxides at the surface. This hydrothermal coating approach is versatile and can be applied not only to NCM materials but also to other electrode materials used in lithium-ion batteries.

The results provide strong evidence that the nano-sized metal oxide coating layer plays a critical role in reducing residual lithium compounds, stabilizing the surface of NCM811, mitigating surface degradation, and suppressing side reactions. Furthermore, this bifunctional coating approach simplifies the manufacturing process and reduces costs by combining two individual processes. These features make it a promising technology for mass production in the cathode materials industry for lithium-ion batteries.

Author Contributions: Conceptualization, material synthesis, characterizations and electrochemical measurements, writing—original draft preparation, methodology, investigation, and resources, S.H.K. and Y.-E.Y.; conceptualization, writing—review and editing, N.M.S.; supervision, funding acquisition, J.-S.K. All authors have read and agreed to the published version of the manuscript.

Funding: This work was supported by the Technology Innovation Program (20018912, 20011928), funded by the Ministry of Trade, Industry and Energy (MOTIE, Republic of Korea).

Data Availability Statement: Data are contained within the article.

Conflicts of Interest: The authors declare no conflicts of interest.

References

- Zhu, X.; Huang, A.; Martens, I.; Vostrov, N.; Sun, Y.; Richard, M.; Schülli, T.; Wan, L. High-voltage spinel cathode materials: Navigating the structural evolution for lithium-ion batteries. *Adv. Mater.* **2024**, *36*, 2403482. [[CrossRef](#)] [[PubMed](#)]
- Feng, N.; Wang, J.; Lin, Y.; Liang, X.; Yang, G. Recycling electrode materials of spent lithium-ion batteries for high-efficiency catalyst application: Recent advances and perspectives. *Eney Fuels* **2024**, *38*, 19174–19187. [[CrossRef](#)]
- Zhao, J.; Zhou, F.; Wang, H.; Qu, X.; Wang, D.; Cai, Y.; Zheng, Z.; Wang, D.; Yin, H. Coupling electrochemical leaching with solvent extraction for recycling spent lithium-ion batteries. *Environ. Sci. Technol.* **2024**, *58*, 16803–16814. [[CrossRef](#)] [[PubMed](#)]
- Ren, K.; Liu, H.; Guo, J.; Sun, X.; Jiang, F.; Guo, C.; Bao, W.; Yu, F.; Kalimuldina, G.; Kong, L.; et al. Working principles of high-entropy electrolytes in rechargeable batteries. *ACS Energy Lett.* **2024**, *9*, 2960–2980. [[CrossRef](#)]
- Wang, J.; Ma, J.; Zhuang, Z.; Liang, Z.; Jia, K.; Ji, G.; Zhou, G.; Cheng, H. Toward Direct regeneration of spent lithium-ion batteries: A next-generation recycling method. *Chem. Rev.* **2024**, *124*, 2839–2887. [[CrossRef](#)]
- Qi, M.; Wang, L.; Huang, X.; Ma, M.; He, X. Surface engineering of cathode materials: Enhancing the high performance of lithium-ion batteries. *Small* **2024**, *20*, 2402443. [[CrossRef](#)]
- Xu, P.; Tan, D.; Jiao, B.; Gao, H.; Yu, X.; Chen, Z. A materials perspective on direct recycling of lithium-ion batteries: Principles, challenges and opportunities. *Adv. Funct. Mater.* **2023**, *33*, 2213168. [[CrossRef](#)]
- Wulandari, T.; Fawcett, D.; Majumder, S.; Poinern, G. Lithium-based batteries, history, current status, challenges, and future perspectives. *Battery Energy* **2023**, *2*, 20230030. [[CrossRef](#)]
- Wang, F.; Bai, J. Synthesis and processing by design of high-nickel cathode materials. *Batter. Supercaps* **2021**, *5*, e202100174. [[CrossRef](#)]
- Zhao, C.; Andersen, P.; Træholt, C.; Hashemi, S. Grid-connected battery energy storage system: A review on application and integration. *Renew. Sustain. Energy Rev.* **2023**, *182*, 113400. [[CrossRef](#)]
- Xu, X.; Han, X.; Lu, L.; Wang, F.; Yang, M.; Liu, X.; Wu, Y.; Tang, S.; Hou, Y.; Hou, J.; et al. Challenges and opportunities toward long-life lithium-ion batteries. *J. Power Sources* **2024**, *603*, 234445. [[CrossRef](#)]
- Rahman, T.; Alharbi, T. Exploring Lithium-Ion Battery Degradation: A concise review of critical factors, impacts, data-driven degradation estimation techniques, and sustainable directions for energy storage systems. *Batteries* **2024**, *10*, 220. [[CrossRef](#)]
- Guo, W.; Fu, D.; Tian, F.; Song, H.; Wang, C. Ca-based hybrid interfaces inhibit uncontrolled electrolyte decomposition for efficient Ion-Storage. *Chem. Eng. J.* **2024**, *489*, 151116. [[CrossRef](#)]
- Jiao, S.; Wang, J.; Hu, Y.; Yu, X.; Li, H. High-Capacity Oxide Cathode beyond 300 mAh/g. *ACS Energy Lett.* **2023**, *8*, 3025–3037. [[CrossRef](#)]
- Zou, K.; Jiang, M.; Ning, T.; Tan, L.; Zheng, J.; Wang, J.; Ji, X.; Li, L. Thermodynamics-directed bulk/grain-boundary engineering for superior electrochemical durability of Ni-rich cathode. *J. Energy Chem.* **2024**, *97*, 321–331. [[CrossRef](#)]
- Gao, X.; Jiang, L.; Lu, X.; Zhou, X.; Li, C.; Shi, J.; Sheng, L. High performance flexible lithium-ion battery anodes: Carbon nanotubes bridging bamboo-shaped carbon-coated manganese oxide nanowires via carbon welding. *J. Alloys Compd.* **2024**, *971*, 172728. [[CrossRef](#)]
- Cho, W.; Lim, Y.J.; Lee, S.; Kim, J.H.; Song, J.; Yu, J.; Kim, Y.; Park, M. Facile Mn surface doping of Ni-rich layered cathode materials for lithium ion batteries. *ACS Appl. Mater. Interfaces* **2018**, *10*, 38915–38921.

18. Liang, J.; Zeng, X.; Zhang, X.; Wang, P.; Ma, J.; Yin, Y.; Wu, X.; Guo, Y.; Wan, L. Mitigating interfacial potential drop of cathode–solid electrolyte via ionic conductor layer to enhance interface dynamics for solid batteries. *J. Am. Chem. Soc.* **2018**, *140*, 6767–6770. [[CrossRef](#)]
19. Pan, H.; Zhang, S.; Chen, J.; Gao, M.; Liu, Y.; Zhu, T.; Jiang, Y. Li-and Mn-rich layered oxide cathode materials for lithium-ion batteries: A review from fundamentals to research progress and applications. *Mol. Syst. Des. Eng.* **2018**, *3*, 748–803.
20. Fan, Q.; Yang, S.; Liu, J.; Liu, H.; Lin, K.; Liu, R.; Hong, C.; Liu, L.; Chen, Y.; An, K. Mixed-conducting interlayer boosting the electrochemical performance of Ni-rich layered oxide cathode materials for lithium ion batteries. *J. Power Sources* **2019**, *421*, 91–99. [[CrossRef](#)]
21. Shao, Y.; Xu, J.; Amardeep, A.; Xia, Y.; Meng, X.; Liu, J.; Liao, S. Lithium-Ion conductive coatings for nickel-rich cathodes for lithium-ion batteries. *Small Methods* **2024**, *8*, 2400256. [[CrossRef](#)] [[PubMed](#)]
22. Sun, T.; Meng, J.; Wang, F.; Chen, C.; Fu, D.; Zhong, Y.; Jin, S.; Dmytro, S.; Zhang, Q.; Ma, Q. The effect of heating rate on microstructure and electrochemical performance of nickel-rich layered oxides cathode materials. *Electrochim. Acta* **2024**, *138*, 15–21. [[CrossRef](#)]
23. Aktekin, B.; Sedykh, A.; Müller-Buschbaum, K.; Henss, A.; Janek, J. The Formation of residual lithium compounds on Ni-RichNCM oxides: Their impact on the electrochemical performance of sulfide-based ASSBs. *Adv. Funct. Mater.* **2024**, *34*, 2313252. [[CrossRef](#)]
24. Yue, M.; Azam, S.; Zhang, N.; Dahn, J.; Yang, C. Residual NMP and Its Impacts on performance of Lithium-Ion Cells. *J. Electrochem. Soc.* **2024**, *507*, 145140. [[CrossRef](#)]
25. Park, K.; Park, J.; Hong, S.; Choi, B.; Seo, S.; Park, J.; Min, K. Enhancement in the electrochemical performance of zirconium/phosphate bi-functional coatings on $\text{LiNi}_{0.8}\text{Co}_{0.15}\text{Mn}_{0.05}\text{O}_2$ by the removal of Li residuals. *Phys. Chem. Chem. Phys.* **2016**, *18*, 29076–29085. [[CrossRef](#)]
26. Välikangas, J.; Laine, P.; Hu, T.; Tynjälä, P.; Selent, M.; Molaiyan, P.; Jürgen, K.; Lassi, U. Effect of secondary heat treatment after a washing on the electrochemical performance of Co-Free $\text{LiNi}_{0.975}\text{Al}_{0.025}\text{O}_2$ cathodes for Li-Ion batteries. *Small* **2024**, *20*, 2305349. [[CrossRef](#)]
27. Wang, D.; Li, X.; Wang, Z.; Guo, H.; Chen, X.; Zheng, X.; Xu, Y.; Ru, J. Multifunctional $\text{Li}_2\text{O}-2\text{B}_2\text{O}_3$ coating for enhancing high voltage electrochemical performances and thermal stability of layered structured $\text{LiNi}_{0.5}\text{Co}_{0.2}\text{Mn}_{0.3}\text{O}_2$ cathode materials for lithium ion batteries. *ACS Appl. Mater. Interfaces* **2022**, *14*, 25490–25500.
28. Yu, Z.; Tong, Q.; Zhao, G.; Zhu, G.; Tian, B.; Cheng, Y. Combining surface holistic Ge Coating and subsurface Mg doping to Enhance the electrochemical performance of $\text{LiNi}_{0.8}\text{Co}_{0.1}\text{Mn}_{0.1}\text{O}_2$ cathodes. *Electrochim. Acta* **2017**, *248*, 534–540. [[CrossRef](#)]
29. Lu, J.; Xu, C.; Dose, W.; Dey, S.; Wang, X.; Wu, Y.; Li, D.; Ci, L. Microstructures of layered Ni-rich cathodes for lithium-ion batteries. *Chem. Soc. Rev.* **2024**, *53*, 4707–4740. [[CrossRef](#)]
30. Wang, M.; Zhang, R.; Gong, Y.; Su, Y.; Xiang, D.; Chen, L.; Chen, Y.; Luo, M.; Chu, M. Improved electrochemical performance of the $\text{LiNi}_{0.8}\text{Co}_{0.1}\text{Mn}_{0.1}\text{O}_2$ material with lithium-ion conductor coating for lithium-ion batteries. *Solid State Ion.* **2017**, *312*, 53–60. [[CrossRef](#)]
31. Chen, H.; Xia, X.; Ma, J. Comprehensive review of Li-Rich Mn-Based layered Oxide cathode materials for lithium-Ion batteries: Theories, challenges, strategies and perspectives. *ChemSusChem* **2024**, *17*, e202401120. [[CrossRef](#)] [[PubMed](#)]
32. Wang, M.; Gong, Y.; Gu, Y.; Chen, Y.; Chen, L.; Shi, H. Effects of fast lithium-ion conductive coating layer on the nickel rich layered oxide cathode material. *Ceram. Int.* **2019**, *45*, 3177–3185. [[CrossRef](#)]
33. Benedetti-Pichler, A.; Cefola, M. Warder's method for the titration of carbonates. *Ind. Eng. Chem. Anal. Ed.* **1939**, *11*, 327–332. [[CrossRef](#)]
34. Zhang, Y.; Song, Y.; Liu, J. Double conductor coating to Improve the structural stability and electrochemical performance of $\text{LiNi}_{0.8}\text{Co}_{0.1}\text{Mn}_{0.1}\text{O}_2$ Cathode Material. *ACS Sustain. Chem. Eng.* **2023**, *11*, 2264–2274. [[CrossRef](#)]
35. Nawaz, R.; Kait, C.F.; Chia, H.Y.; Isa, M.H.; Huei, L.W. Glycerol-mediated facile synthesis of colored titania nanoparticles for visible light photodegradation of phenolic compounds. *Nanomaterials* **2019**, *9*, 1586. [[CrossRef](#)]
36. Feng, S.; Li, X.; Shang, C.; Tang, L.; Zhang, J. Germanium based glass modified by graphene as anode material with high capacity for lithium-ion batteries. *J. Non Cryst. Solids* **2024**, *646*, 123257. [[CrossRef](#)]
37. Reddy, P.H.; Kir'yanov, A.; Dhar, A.; Das, S.; Dutta, D.; Pal, M.; Barmenkov, Y.; Minguella-Gallardo, J.; Bhadra, S.K.; Paul, M.C. Fabrication of ultra-high numerical aperture GeO_2 -doped fiber and its use for broadband supercontinuum generation. *Appl. Opt.* **2017**, *56*, 9315–9324. [[CrossRef](#)]
38. Tang, M.; Yang, J.; Chen, N.; Zhu, S.; Wang, X.; Wang, T.; Zhang, C.; Xia, Y. Overall structural modification of a layered Ni-rich cathode for enhanced cycling stability and rate capability at high voltage. *J. Mater. Chem. A* **2019**, *7*, 6080–6089. [[CrossRef](#)]
39. Wang, Q.; Yang, S.; Miao, J.; Zhang, Y.; Zhang, D.; Chen, Y.; Li, Z. Synthesis of graphene supported $\text{Li}_2\text{SiO}_3/\text{Li}_2\text{SnO}_3$ anode material for rechargeable lithium-ion batteries. *Appl. Surf. Sci.* **2019**, *469*, 253–261. [[CrossRef](#)]
40. Bandpey, M.; Dorri, M.; Babaei, A.; Zamani, C.; Bortolotti, M. Improved electrochemical performance of the cation-disordered NMC cathode of Lithium-Ion batteries by lithium phosphate coating. *ACS Appl. Energy Mater.* **2023**, *6*, 7974–7984. [[CrossRef](#)]

41. Li, X.; Zhao, Z.; Deng, Y.; Ouyang, D.; Yang, X.; Chen, S.; Liu, P. Interfacial engineering in SnO₂-embedded graphene anode materials for high performance lithium-ion batteries. *Sci. Rep.* **2024**, *16*, 1–10. [[CrossRef](#)]
42. Wang, C.; Liu, F.; Kan, K.; Zhao, P.; Xiong, C. Realization of a high voltage Ni rich layer LiNi_{0.5}Co_{0.2}Mn_{0.3}O₂ single crystalline cathode for LIBs by surface modification. *Ceram. Int.* **2023**, *49*, 7956–7964. [[CrossRef](#)]

Disclaimer/Publisher’s Note: The statements, opinions and data contained in all publications are solely those of the individual author(s) and contributor(s) and not of MDPI and/or the editor(s). MDPI and/or the editor(s) disclaim responsibility for any injury to people or property resulting from any ideas, methods, instructions or products referred to in the content.